

## ARTICLES

**Comparative Investigation of Energy Relaxation Dynamics of Gold Nanoparticles and Gold–Polypyrrole Encapsulated Nanoparticles****Hyun Jong Shin, In-Wook Hwang, Young-Nam Hwang, and Dongho Kim\****National Creative Research Initiatives Center for Ultrafast Optical Characteristics Control and Department of Chemistry, Yonsei University, Seoul 120-749, Korea***Seon Hee Han and Jae-Suk Lee***Department of Materials and Engineering, Kwangju Institute of Science and Technology, Kwangju 500-712, Korea***Gyoujin Cho***Department of Chemical Engineering, Sunchon National University, 315 Maegok, Sunchon, Chonnam 540-742, Korea**Received: September 12, 2002; In Final Form: January 3, 2003*

We report the femtosecond transient absorption dynamics of the gold and gold–polypyrrole nanoparticles by photoexcitation at various wavelengths. The bleach recovery dynamics of the surface plasmon band for the gold and gold–polypyrrole nanoparticles exhibit different responses to the pump beam energy and intensity in thermal energy transfer from the gold nanoparticles to the surrounding medium or embedding material. This indicates that directly attached polypyrroles provide fast thermal energy transfer pathways for the core gold nanoparticles.

**Introduction**

During the past decade, nanometer ( $10^{-9}$  m) scaled materials have gained much attention owing to unique properties induced by their high surface-to-volume ratio.<sup>1</sup> These materials often display the intermediate properties between the bulk and the atom, arising from quantum confinement effects.<sup>1–3</sup> Especially, gold and silver nanoparticles as well as nanorods have been investigated to reveal their unique optical, electrical, and photocatalytic properties depending on their sizes and aspect ratios.<sup>1</sup>

Small gold nanoparticles of 5–50 nm diameters have a characteristic surface plasmon absorption band, which arises from a collective oscillation of conduction band electron gases by applied optical and electric field.<sup>3–5</sup> The spectral position and width of surface plasmon absorption of gold nanoparticles is varied by the function of dielectric constant of surrounding medium or embedding material. Therefore, we can control their absorption position and shape by suitable choice of the dielectric medium.<sup>1,6</sup> Because the surface plasmon band is sensitive to the electron thermal motions and the lattice temperature, the thermalization dynamics in gold nanoparticles have been investigated by monitoring the bleach recovery of the collective electron oscillations in femtosecond pump–probe experiments.<sup>5,7–9</sup> The nonradiative relaxation dynamics in the bare gold nanoparticles can be explained by the two temperature

model (TTM).<sup>9–11</sup> Upon photoexcitation by femtosecond optical pulses, the electrons are heated instantaneously up to several thousands Kelvin and create hot electron gases. The Fermi electron distribution is attained within  $\sim 0.5$  ps through an intrinsic electron–electron scattering process.<sup>9–11</sup> Simultaneously, through electron–phonon interactions, the electron gases are cooled in a few ps until the lattice temperature becomes equilibrated with the electrons. As a consequence, the two relaxation processes cannot be separated as expected from the TTM.<sup>9–11</sup> The nonradiative relaxation process is completed through phonon–phonon interactions with the surrounding medium or embedding materials in the time scale of  $\sim 100$  ps.<sup>1</sup> However, the lifetime of photoexcited gold nanoparticles exhibits the dependence on the incident light intensity and increases linearly as the pump beam intensity increases.<sup>1</sup> This phenomenon can be explained by the fact that higher pump laser power gives higher initial electron temperature and electron heat capacity depends on the electron temperature. Therefore, the overall relaxation processes including electron–phonon and phonon–phonon interactions become slower with increasing the incident light intensity.<sup>1,6,11,12</sup>

Moreover, Varnavski et al.<sup>13</sup> reported the emission from the gold nanoparticles encapsulated by dendrimer. In their experiment, the dendrimer plays a key role in the relaxation dynamics as a thermal reservoir. Through the coupling of emission dipole moments between the host dendrimer and the encapsulated gold nanoparticle, the dendrimer provides the nonradiative relaxation

\* To whom correspondence should be addressed. Fax: +82-2-2123-2434. E-mail: dongho@yonsei.ac.kr.

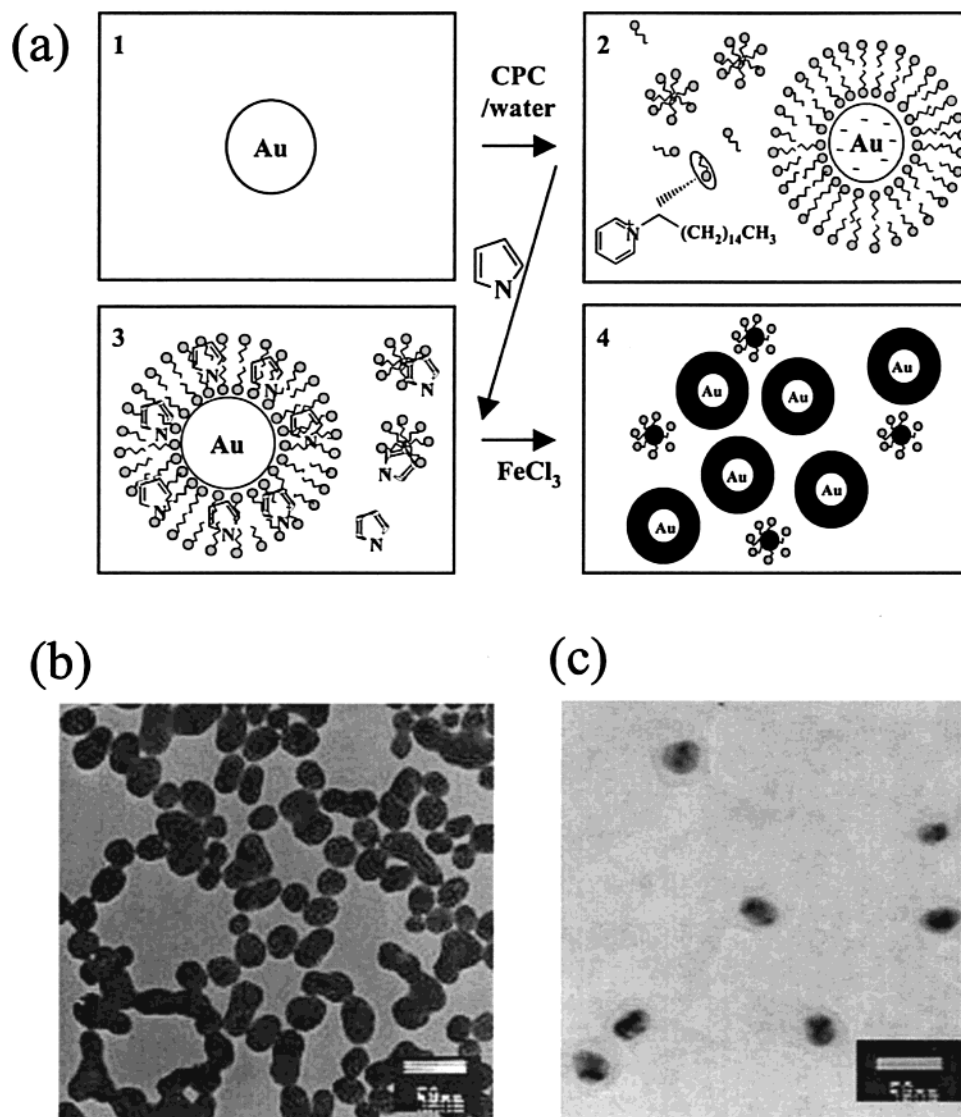


**Figure 1.** The sample preparation scheme for the gold–polypyrrole nanoparticles (a), TEM images of the bare gold (b) and gold–polypyrrole nanoparticles (c) with an average diameter of 25 nm.

channels.<sup>13</sup> As a consequence, the encapsulated gold nanoparticles exhibit faster decay, in addition to the long-lived component with a characteristic lifetime of the host dendrimer.

In our experiment, we compared the relaxation dynamics of the bare gold nanoparticles and polypyrrole encapsulated gold nanoparticles with various photoexcitation energies to investigate the contribution of the interband transition in the surface plasmon relaxation dynamics by femtosecond pump–probe technique. In the bulk gold, the interband transition from the d-band to the Fermi level requires the energy of 2.4 eV and this value could be applied to the 25 nm gold nanoparticles.<sup>6–7,14,15</sup> Therefore, after photoexcitation at 400 nm, the interband transition from the d-band to the conduction band can occur along with the intraband transition.<sup>16</sup> Moreover, since the energy relaxation dynamics of photoexcited metal nanoparticles are sensitive to the electron thermal motion and the lattice temperature, the efficiency of thermal energy transfer from the gold nanoparticles to the surrounding medium or embedding material affects significantly the bleach recovery dynamics.<sup>17</sup> Therefore, to obtain a deep understanding on the energy transfer process from photoexcited gold nanoparticles, a well-known conducting polymer polypyrrole is employed as a thermal reservoir in our experiment.

## Experimental Section

The gold nanoparticles were prepared by the citrate reduction method.<sup>18</sup> In detail, 10 mL of gold chloride trihydrate solution containing 5 mg of Au was added to 85 mL of water ( $>18\text{ M}\Omega$ ) in a 500 mL round-bottom flask equipped with a condenser and stirred vigorously. Five milliliters of 1% sodium citrate solution was added rapidly at the boiling stage. It turned to wine-purple in color after a minute after first turning black. Boiling was continued for 30 min. When the colloidal gold solution reached room temperature, it was stored in a dark bottle and used within a month after preparation. The size of the gold clusters depends on the amount of acid and sodium citrate used during the preparation.

In the case of the encapsulated gold nanoparticles, the bare gold nanoparticles prepared by citrate-induced reduction were used as core material. A brief sample preparation scheme is shown in Figure 1a. CPC (cetylpyridinium chloride), a cationic surfactant, was added to 10 mL of colloidal gold solution, and the mixture was stirred by hand shaking to facilitate the adsorption onto the colloidal gold surface. It formed the micelles in aqueous solution several hours later. Pyrrole or 3-hexylthiophene was added to this solution as a polymerizable

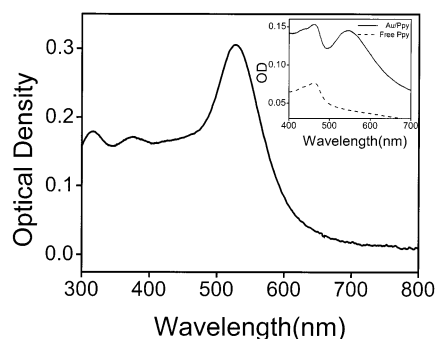


**Figure 2.** The absorption spectrum of the bare gold nanoparticles ( $d = 25$  nm) with a surface plasmon band at 525 nm. Inset shows the absorption spectra of the gold-polypyrrole nanoparticles with a surface plasmon band at (—) 545 nm and (---) free polypyrroles.

monomer, and then diffused in the layer of CPC. Iron(III) chloride initiator was added at least 6 h later, and the solution turned black slowly. To separate out gold-polypyrrole core-shell particles from free polypyrroles, a centrifuge process was necessary. Proper conditions are 8000–10000 rpm for 10 min. The average size of the prepared gold nanoclusters was  $\sim 25$  nm as characterized by TEM (transmission electron microscopy, JEOL JEM-2000FX II), UV-vis (Cary 3 Bio UV-vis spectrophotometer), and light scattering (Malvern Instrument PCS). TEM images of the prepared gold and gold-polypyrrole nanoparticles are shown in Figure 1b,c.

To measure the femtosecond transient absorption change, we utilized a regenerative amplified mode-locked Ti:sapphire laser (800 nm, 100 fs, and 1 kHz). For second-harmonic generation, a 1 mm thick  $\beta$ -BBO crystal was used. The femtosecond continuum pulses were generated in a 1 cm flowing cell containing water and were divided into probe and reference beams. After the OD change of the gold nanoparticles photoexcited at 400, 565, and 600 nm was probed, the delayed continuum pulses passed through band-pass filters centered at 475, 530, and 585 nm with 10 nm bandwidth for each excitation pulse.<sup>19</sup> From the cross-correlation function between the excitation and probe pulses, the full width at half-maximum (fwhm) was estimated to be  $\sim 250$  fs. The time resolution of  $\sim 100$  fs was obtained by the deconvolution of bleach recovery profile with the cross-correlation function with  $\sim 250$  fs in fwhm. Upon the processing of the output current from two photodiodes with a boxcar averager, the probe beam was normalized by the reference beam with pulse-to-pulse configuration. In the transient absorption experiment, the colloidal gold nanoparticles were prepared in a 2 mm quartz cell and checked for the absence of any noticeable change due to photodegradation. The photoexcitation density was also kept as low as possible, which was in the range of several tens of  $\mu\text{J}/\text{cm}^2$ .

## Results

The steady-state absorption spectra of the bare gold nanoparticles and gold-polypyrrole nanoparticles with 25 nm diameter are shown in Figure 2. The surface plasmon absorption bands for the bare gold and gold-polypyrrole nanoparticles are observed at 525 and 545 nm, respectively. The surface plasmon band of the gold-polypyrrole nanoparticles exhibits a  $\sim 20$  nm red shift as well as bandwidth broadening, and the absorbance also decreases by half in comparison with that of the bare gold nanoparticles. The changes in the steady-state absorption spectrum of the gold-polypyrrole nanoparticles are due to the difference in the dielectric constant of the surrounding medium and embedding material. To investigate the electronic transition

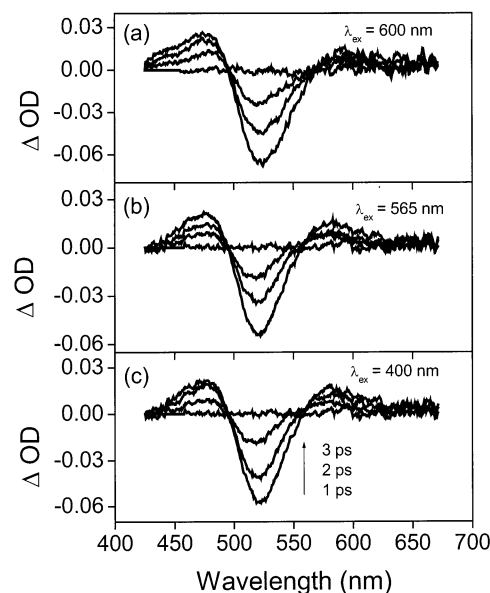


**Figure 3.** A series of chirp-corrected femtosecond transient absorption spectra of the gold nanoparticles during  $\sim 3$  ps time interval immediately after photoexcitation at (a) 600, (b) 565, and (c) 400 nm.

and relaxation dynamics of the bare gold nanoparticles, we have employed the femtosecond transient absorption technique. Figure 3 shows the chirp-corrected transient absorption spectra of the bare gold nanoparticles at various time delays after photoexcitation at 400, 565, and 600 nm. The photoinduced transient absorption bands as well as the bleach peak gradually decrease as the time delay between the pump and probe pulses increases without any noticeable change in spectral features as evidenced by the appearance of two isosbestic points at 494 and 560 nm. The photoinduced transient absorption at both wings of the strong bleach band at 525 nm exhibits an instantaneous buildup within  $\sim 1$  ps. These two photoinduced transient absorption bands are the result of broadening of the surface plasmon band due to the increase of electron temperature and change of dielectric constant of the gold nanoparticles by the strong pump beam intensity.<sup>12</sup>

To gain further insight into the energy relaxation dynamics of the bare gold nanoparticles, the temporal profiles of the bleach recovery by photoexcitation at 400, 565, and 600 nm were monitored at 523 nm (not shown). The bleach recovery is composed of three processes, viz, electron-electron interactions with subpicosecond, electron-phonon interactions with a few picosecond, and finally phonon-phonon interactions with hundreds of picosecond time scales. The bleach recovery by photoexcitation at 400, 565, and 600 nm exhibits nearly the same time constant of  $\sim 1.5$  ps for electron-phonon interactions under the lowest excitation intensity to be at the same electron temperature. This feature is in a good accordance with the results by Link et al.<sup>7</sup>

Since the energy relaxation dynamics is completed through phonon-phonon interactions with the embedding material or surrounding medium with the time constant of hundreds of picosecond, the encapsulated nanoparticles are expected to exhibit different pathways from the bare gold nanoparticles in the energy relaxation dynamics for both thermally and non-thermally excited electrons.<sup>17</sup> In recent works by Varnavski et al.,<sup>13</sup> organic materials act as a thermal reservoir and influence the energy relaxation dynamics of the metal nanoparticles. In this system, the photoluminescence arises from the organic material and is enhanced by the metal surface with a similar mechanism to SERS.<sup>3,13</sup>

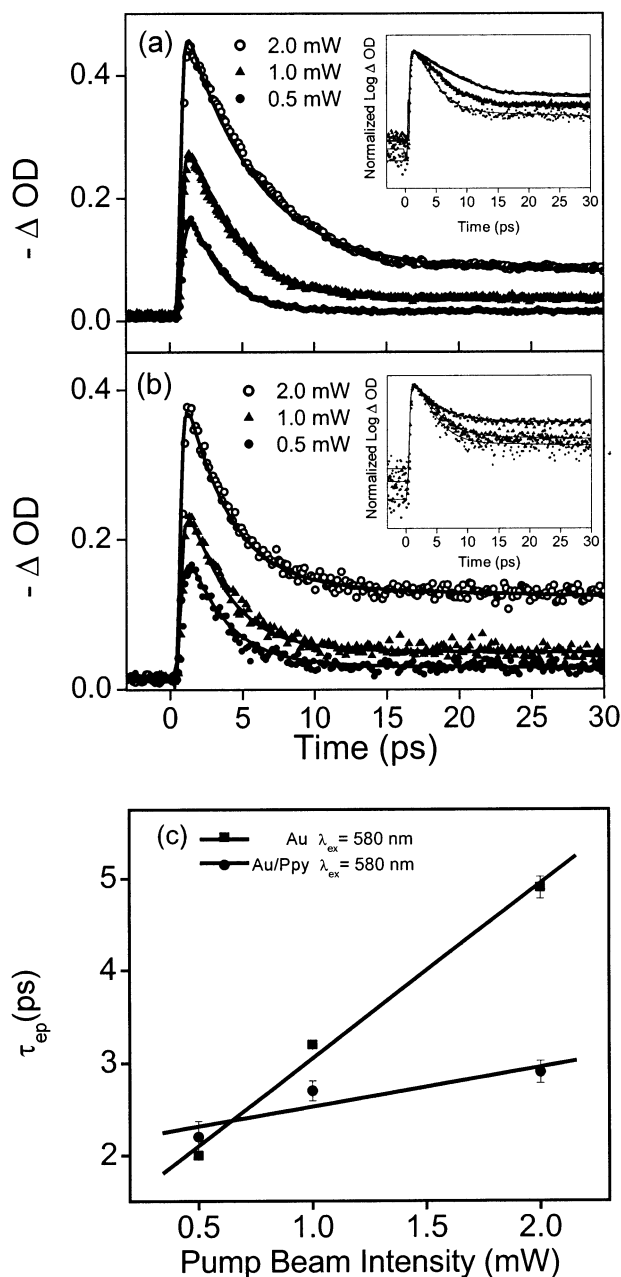


**Figure 4.** The bleach recovery dynamics at 530 nm of the (a) bare gold nanoparticles and (b) gold-polypyrrole nanoparticles with  $d = 25$  nm by photoexcitation at 580 nm with increasing the pump beam intensity. (a) The decay profiles are well fitted by the time constants of 2.0, 3.2, and 4.9 ps with increasing the pump beam intensity. (b) The decay profiles are well fitted by the time constants of 2.2, 2.7 and 2.9 ps with increasing the pump beam intensity. The insets show the normalized logarithmic scale plot. (c) The plot of the time constants for electron-phonon interactions of the (■) bare gold nanoparticles and (●) gold-polypyrrole nanoparticles versus photoexcitation intensity.

To investigate the effect of energy transfer into the surrounding medium or embedding material on the energy relaxation process, the dependence on the pump beam intensity of the bleach recovery dynamics at 530 nm of the bare gold (Figure 4a) and gold-polypyrrole nanoparticles (Figure 4b) by photoexcitation at 580 nm was monitored. According to Figure 2, the absorbance of the gold-polypyrrole nanoparticles is reduced to nearly a half of that of the bare gold nanoparticles and polypyrroles also contribute to the absorbance at 580 nm by  $\sim 10\%$  of the total absorbance. Therefore, in sample preparation,

**TABLE 1: The Lifetimes of the Bleach Recoveries at 530 nm of the Gold and Gold-Polypyrrole Nanoparticles with Various Intensities by Photoexcitation at 400 and 580 nm**

sample	$\lambda_{ex}$ (nm)	$\lambda_{pr}$ (nm)	pump power (mW)	$\tau_1$ (ps) rise	$\tau_2$ (ps) (%) decay	$\tau_3$ (ps) (%) decay
Au bare	580	530	0.5	$\sim 0.4$	2.0 (95)	$\sim 100$ (5)
			1.0	$\sim 0.4$	3.2 (92)	$\sim 200$ (8)
			2.0	$\sim 0.4$	4.9 (84)	$\sim 200$ (26)
	400	530	0.5	$\sim 0.4$	1.3 (99)	$< 100$ (1)
			1.0	$\sim 0.4$	2.0 (95)	$\sim 100$ (5)
			2.0	$\sim 0.4$	2.7 (93)	$\sim 100$ (7)
Au/Ppy	580	530	0.5	$\sim 0.5$	2.2 (93)	$\sim 100$ (7)
			1.0	$\sim 0.6$	2.7 (87)	$\sim 200$ (13)
			2.0	$\sim 0.7$	2.9 (71)	$\sim 200$ (29)
	400	530	0.5	$\sim 0.3$	1.4 (97)	$\sim 100$ (3)
			1.0	$\sim 0.3$	2.1 (94)	$\sim 200$ (6)
			2.0	$\sim 0.3$	2.5 (89)	$\sim 200$ (11)

<sup>a</sup> These values stand for the ratio of phonon-phonon and electron-phonon interactions written in the percentage value of  $A_3/(A_2 + A_3)$ .

the OD value of the gold-polypyrrole nanoparticles was adjusted to have the same initial electron temperature by photoexcitation at 580 nm as that of the bare gold nanoparticles, which is the same absorbance by the core gold nanoparticles in the gold-polypyrrole nanoparticles at 580 nm as that of the bare gold nanoparticles. In the bleach recovery at 530 nm, both the bare gold and gold-polypyrrole nanoparticles exhibit an increment in the time constants for electron-phonon interactions with an increase of the 580 nm pump beam intensity (Figure 4 and Table 1). However, the time constants for electron-phonon interactions of the bare gold nanoparticles are more sensitive to the pump beam intensity than those of the encapsulated gold nanoparticles as shown in Figure 4c. In the case of the bare gold nanoparticles, the time constants for electron-phonon interactions become larger from 2.0 to 4.9 ps, whereas the encapsulated gold nanoparticles exhibit negligible change in their time constants from 2.2 to 2.9 ps as the pump beam intensity increases at 580 nm (Figure 4c, Table 1). The amplitudes for phonon-phonon interactions in the bleach recovery signal of both the bare gold and gold-polypyrrole nanoparticles largely increase as the pump beam intensity increases as shown in Figure 4 and Table 1. According to Figure 2, polypyrroles contribute to about  $\sim 10\%$  of the total absorbance of the gold-polypyrrole nanoparticles at 530 nm. Since photoexcited polypyrroles exhibit an instantaneous rise and a long lifetime ( $\sim 1$  ns) in the energy relaxation process, about  $\sim 10\%$  of the amplitude for phonon-phonon interactions in the total bleaching signal of the gold-polypyrrole nanoparticles at 530 nm may be regarded as being due to the existence of the polypyrroles.

We also investigated the pump power dependence on the bleach recovery of the bare gold (Figure 5a) and gold-polypyrrole nanoparticles (Figure 5b) with a photoexcitation at 400 nm to investigate the effect of the interband transition from the d-band to the conduction band. As shown in the inset of Figure 2, polypyrroles also contribute to the absorbance at 400 nm by nearly a half of the total absorbance. Therefore, in sample preparation, the OD value of the gold-polypyrrole nanoparticles was adjusted to exhibit the same initial electron temperature with photoexcitation at 400 nm as that of the bare gold nanoparticles at 400 nm as that of the bare gold nanoparticles after subtracting the absorbance of polypyrroles in the gold-polypyrrole nanoparticles. The time constants for electron-phonon interactions of the bare gold and gold-polypyrrole nanoparticles in the bleach recovery signals at 530 nm by



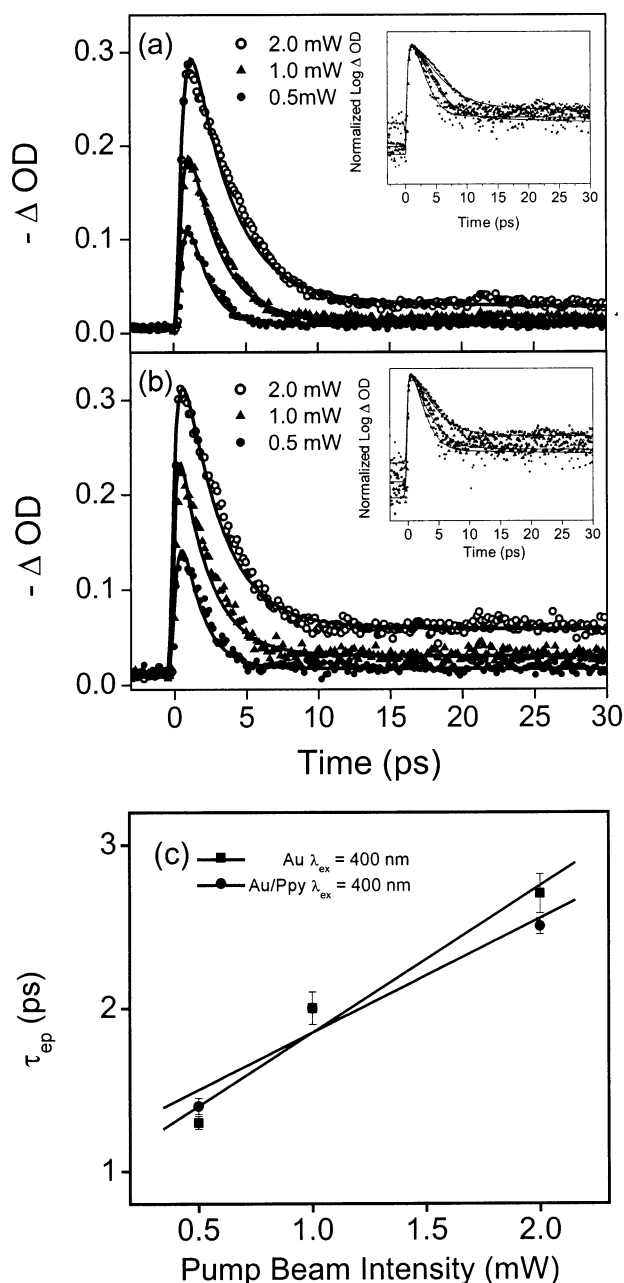


**Figure 5.** The bleach recovery dynamics at 530 nm of the (a) bare gold nanoparticles and (b) gold-polypyrrole nanoparticles with  $d = 25$  nm by photoexcitation at 400 nm with increasing the pump beam intensity. (a) The decay profiles are well fitted by the time constants of 1.3, 2.0 and 2.7 ps with increasing the pump beam intensity. (b) The decay profiles are well fitted by the time constants of 1.4, 2.1 and 2.5 ps with increasing the pump beam intensity. The insets show the normalized logarithmic scale plot. (c) The plot of the time constants for electron-phonon interactions of the (■) bare gold nanoparticles and (●) gold-polypyrrole nanoparticles versus photoexcitation intensity.

photoexcitation at 400 nm exhibit similar responses to the pump beam intensity as shown in Figure 5c and Table 1. The time constants for electron-phonon interactions of the bare gold nanoparticles change from 1.3 to 2.7 ps, and those of the encapsulated gold nanoparticles change from 1.4 to 2.5 ps with an increase of the 400 nm pump beam intensity (Figure 5c and Table 1). Moreover, in both the bare gold and gold-polypyrrole nanoparticles, phonon-phonon interactions in the bleach recovery signals at 530 nm are slightly enhanced in their amplitudes as the 400 nm pump beam intensity increases (Figure

5 and Table 1). Since polypyrroles absorb light significantly near 400 nm (inset of Figure 2), it is likely that polypyrroles themselves participate in the photoexcitation dynamics especially upon photoexcitation at 400 nm.

## Discussion

To explain the overall photoexcitation dynamics of nanoparticles, we employed the modified TTM. According to the TTM, the bleach recovery can be described by the following equation.<sup>1,9,15</sup>

$$A(t) = A_{NT} \exp[-(t - t_0)/t_{NT}] + A_T \exp[(t - t_0)/\tau_{ep}] \{1 - \exp[-(t - t_0)/\tau_{ee}]\}$$

In this equation,  $A(t)$  stands for the magnitude of absorption change at a given time  $t$  and  $A_{NT}$  and  $A_T$  represent the nonthermal and thermal absorption processes, respectively.  $\tau_{ee}$  and  $\tau_{ep}$  represent electron-electron and electron-phonon interactions, respectively. Upon the application of this equation to the bleach recovery dynamics of the bare gold nanoparticles, the TTM yields the time constants of 0.3–0.4 ps and 1.6–3.3 ps for electron-electron and electron-phonon interactions depending on the excitation intensity, respectively.<sup>15</sup> The calculated values are similar to our experimental results of 0.1–0.5 ps and 1.3–4.9 ps for the bleach recovery processes through electron-electron and electron-phonon interaction processes. In addition, the spectral shape and the amplitude of each interaction in the relaxation dynamics changes as the pump beam intensity increases.

The energy of photoexcitation at 580 nm excites the free carriers in the conduction band. Optically excited electrons create nonthermal distribution and the electron gas thermalizes within  $\sim 1$  ps via electron-electron and electron-phonon scattering.<sup>6</sup> During the thermalization process, the excess energy of optically excited electrons is redistributed among the conduction band electrons via phonon emission until the electron and lattice temperatures are equal.<sup>15</sup> Since lattice transfers its thermal energy to the surrounding medium or embedding material via phonon-phonon interactions, the amplitudes for phonon-phonon interactions are likely to change efficiently with a change in the pump beam intensity. As seen in Figure 4, as expected, phonon-phonon interactions are largely enhanced with an increase of the pump beam intensity. Moreover, the increments in the time constants for electron-phonon interactions of the bare gold nanoparticles are much larger than those of the gold-polypyrrole nanoparticles (Figure 4c and Table 1). Because polypyrroles are directly attached to the gold nanoparticles, the excess energy by the increased pump beam intensity is efficiently dissipated to the directly attached polypyrroles via phonon-phonon interaction. Therefore, the lattice temperature cools faster than that of the bare gold nanoparticles and the time constants for electron-phonon interactions exhibit negligible change with an increase of the pump beam intensity (Figure 4c and Table 1). On the other hand, since the gold nanoparticles transfer their excess energy only to the surrounding medium via phonon-phonon interactions, the energy transfer rates depend on the diffusion rate of the surrounding medium. Thus, the excess thermal energy in the gold lattice is not vanished efficiently and consequently affects the time constants for electron-phonon interactions in the bare gold nanoparticles.

At the photoexcitation energy of 400 nm, polypyrroles absorb nearly the same amount of photons as the core gold nanoparticles as shown in the inset of Figure 2. Therefore, photoexcited polypyrroles cannot provide efficient thermal energy

relaxation channels to the gold nanoparticles. As a result, the bleach recoveries of the surface plasmon at 530 nm for the bare gold and gold–polypyrrole nanoparticles by photoexcitation at 400 nm exhibit nearly the same time constants for electron–phonon interactions. Moreover, considering additional contribution by photoexcited polypyrroles to the overall bleach recovery signal at 530 nm in the gold–polypyrrole nanoparticles, the enhancement in the amplitude for phonon–phonon interactions with an increase of the pump beam intensity is considered to be even less. Therefore, we can conclude that the amplitude changes for phonon–phonon interactions are negligible (Figure 5). For this reason, in the bleach recovery process by photoexcitation at 400 nm, the time constants for electron–phonon interactions and the amplitudes for phonon–phonon interactions do not exhibit any significant effect of encapsulation.

## Conclusion

In the present work, we have investigated the thermal energy relaxation dynamics of the gold and gold–polypyrrole nanoparticles by changing the excitation energies and intensities. Upon photoexcitation at 580 nm, the time constants for electron–phonon interactions of the gold nanoparticles significantly increase as the pump beam intensity increases. On the contrary, the gold–polypyrrole nanoparticles exhibit negligible changes in the time constants for electron–phonon interactions with an increase in the pump beam intensity. In addition, the amplitudes for phonon–phonon interactions of the gold–polypyrrole nanoparticles are enhanced significantly with an increase of the pump beam intensity at 580 nm in contrast with a negligible enhancement in the bare gold nanoparticles. These features illustrate that directly attached polypyrroles provide efficient channels for the thermal energy relaxation to the core gold nanoparticles in the polypyrrole encapsulated gold nanoparticles.

On the other hand, upon photoexcitation at 400 nm, polypyrroles in the gold–polypyrrole nanoparticles can be excited directly due to relatively strong absorbance at 400 nm. Thus, photoexcited polypyrroles cannot act as an efficient thermal reservoir. Consequently, the overall photoexcitation dynamics

of the gold and gold–polypyrrole nanoparticles by photoexcitation at 400 nm are nearly the same regardless of the changes in the excitation intensity.

**Acknowledgment.** The work at Yonsei University has been financially supported by the Creative Research Initiatives Program of the Ministry of Science and Technology of Korea. One of the authors (J.S.L.) thanks the financial support by the BK21 program.

## References and Notes

- (1) Link, S.; El-Sayed, M. A. *J. Phys. Chem. B* **1999**, *103*, 8410.
- (2) Link, S.; El-Sayed, M. A. *J. Phys. Chem. B* **1999**, *103*, 4212.
- (3) Wilcoxon, J. P.; Martin, J. E.; Parsapour, F.; Wiedenman, B.; Kelley, D. F. *J. Chem. Phys.* **1998**, *108*, 9137.
- (4) Kittel, C. *Introduction to Solid State Physics*; Wiley: New York, 1996.
- (5) Ahmadi, T. S.; Longunov, S. L.; El-Sayed, M. A. *J. Phys. Chem.* **1996**, *100*, 8053.
- (6) Perner, M.; Bost, P.; Lemmer, U.; Plessen, G.; Feldmann, J.; Becker, U.; Mennig, M.; Schmitt, M.; Schmidt, H. *Phys. Rev. Lett.* **1997**, *78*, 2192.
- (7) Link, S.; Burda, C.; Wang, Z. L.; El-Sayed, M. A. *J. Chem. Phys.* **1999**, *111*, 1255.
- (8) Logunov, S. L.; El-Sayed, M. A.; Khoury, J. T.; Whetten, R. L. *J. Phys. Chem. B* **1997**, *101*, 3713.
- (9) Sun, C.-K.; Vallée, F.; Acioli, L. H.; Ippen, E. P.; Fujimoto, J. G. *Phys. Rev. B* **1993**, *48*, 12365.
- (10) Sun, C.-K.; Vallée, F.; Acioli, L. H.; Ippen, E. P.; Fujimoto, J. G. *Phys. Rev. B* **1994**, *50*, 15337.
- (11) Groeneveld, R. H.; Sprik, R.; Lagendijk, A. *Phys. Rev. B* **1995**, *51*, 11433.
- (12) Hodak, J. H.; Henglein, A.; Hartland, G. V. *J. Chem. Phys.* **1999**, *111*, 8613.
- (13) Varnavski, O.; Ispasoiu, R. G.; Balogh, L.; Tomalia, D.; Goodson, T., III. *J. Chem. Phys.* **2001**, *114*, 1962.
- (14) Marcos, M.; Alvarez, J. T.; Khoury, T.; Gregory S.; Marat, N. S.; Shafigullin, I. V.; Robert, L. W. *J. Phys. Chem. B* **1997**, *101*, 3706.
- (15) Hwang, Y.-N.; Jeong, D. H.; Shin, H. J.; Kim, D.; Jeoung, S. C.; Han, S. H.; Lee, J.-S.; Cho, G. *J. Phys. Chem. B* **2002**, *106*, 7581.
- (16) Cracknell, A. P. In *Numerical Data and Functional Relationships in Science and Technology*; Hellwege, K.-H., Olsen, J. L., Eds.; Landolt-Börnstein New Series Group III.; Springer-Verlag: Berlin, 1984; Vol. 13C, p 48.
- (17) Link, S.; Furube, A.; Mohamed, M. B.; Asahi, T.; Masuhara, H.; El-Sayed, M. A. *J. Phys. Chem. B* **2002**, *106*, 945.
- (18) Turkevich, J.; Garton, G.; Stevenson, P. C.; Hillier, J. *Discuss. Faraday Soc.* **1951**, *11*, 55.
- (19) Klimov V. I.; McBranch, D. W. *Opt. Lett.* **1998**, *23*, 277.